

A Microneedle Technology for Sampling and Sensing Bacteria in the Food Supply Chain

Doyoon Kim, Yunteng Cao, Dhanushkodi Mariappan, Michael S. Bono Jr., A. John Hart, and Benedetto Marelli*

Food quality monitoring, particularly, the detection of bacterial pathogens and spoilage throughout the food supply chain, is critical to ensure global food safety and minimize food loss. Incorporating sensors into packaging is promising, but it is challenging to achieve the required sampling volume while using food-safe sensor materials. Here, by leveraging water-based processing of silk fibroin, a platform for the detection of pathogenic bacteria in food is realized using a porous silk microneedle array; the microneedle array samples fluid from the interior of the food by capillary action, presenting the fluid to polydiacetylene-based bioinks printed on the backside of the array. Through the colorimetric response of bioink patterns, *Escherichia coli* contamination in fish fillets is identified within 16 h of needle injection. This response is distinct from spoilage measured via the increase in sample pH. It is also shown that the microneedles can pierce commercial food packaging, and subsequently sample fluid and present it to the sensor, enabling the adaptation of the technology downstream in food supply chains such as in stores or at home. This study highlights that regenerated structural biopolymers can serve as safe materials for food contact and sensing with robust mechanical properties and tailored chemistry.

1. Introduction

Food safety is a major threat to public health and well-being of society.^[1] The World Health Organization (WHO) estimates that foodborne contamination kills 420 000 people per year worldwide.^[1,2] In the United States, according to the Centers for Disease Control and Prevention (CDC), roughly 1 in 6 people gets sick, 128 000 are hospitalized, and 3000 die of foodborne diseases each year.^[3] The CDC also estimates that the cost of foodborne diseases amounts to more than \$15.6 billion each year. Increasing the efficiency of the food supply chain is also


a priority to avoid the current loss of circa one third of the global food production.^[4] The US National Resources Defense Council estimates that 40% of the food produced in America goes uneaten. This translates to about \$218 billion worth of food that is wasted every year.^[5] In the case of fresh produce, it has been shown that more than 80% of American consumers misinterpret date labels and throw food away prematurely due to concerns regarding safety. Predetermined expiration labels also increase the public distrust in food safety and result in broad food recalls in the event of contaminations and in an increased use of food preservatives by producers to extend product shelf-life.^[1,6–8]

To overcome these challenges, substantial progress has been made toward the design of smart food labeling that provides real-time quality information,^[1,9] such as by incorporating indicators that monitor and report information on CO₂ concentration,^[10] pH,^[11] humidity,^[12] and storage

temperature.^[13] In addition, active packaging materials have been suggested to prevent changes in the food quality by radically scavenging oxidation reactions of food.^[14,15] Despite these advances, monitoring the presence of pathogenic microorganisms such as *Escherichia coli* O157:H7 and *Salmonella Typhimurium* remains an open challenge. Conventional microbial detection technologies, based on polymerase chain reaction (PCR) and standard cell culture techniques, are generally applied in the food supply chain at the processing and storage/transportation level to meet quality control requirements.^[16] These microbial analyses involve sophisticated laboratory equipment and professional operations and are disruptive, time consuming, and expensive.^[1,17,18] To overcome these challenges, there has been a recent focus on the development of new techniques to accelerate microbial analysis while enhancing resolution, precision, and accuracy. Combinations of microfluidic devices with optical sensors,^[18] fluorogenic probes,^[19] or electrogenerated chemiluminescences^[20] are examples of such approach. For example, Yousefi et al. reported a microarray of RNA-cleaving fluorogenic DNzyme probe printed on a flexible and transparent film for detection of *E. coli* in meat and apple juice.^[19] Development of low-cost attachments for portable devices such as smartphones has further increased the practicability of sensors that use fluorescence signals as reporter.^[21]

Dr. D. Kim, Y. Cao, Prof. B. Marelli
Department of Civil and Environmental Engineering
Massachusetts Institute of Technology
77 Massachusetts Ave, Cambridge, MA 02139-4307, USA
E-mail: bmarelli@mit.edu

Dr. D. Mariappan, Dr. M. S. Bono Jr., Prof. A. J. Hart
Department of Mechanical Engineering
Massachusetts Institute of Technology
77 Massachusetts Ave, Cambridge, MA 02139-4307, USA

 The ORCID identification number(s) for the author(s) of this article can be found under <https://doi.org/10.1002/adfm.202005370>.

DOI: 10.1002/adfm.202005370

Nonetheless, these methods require portable devices analyzing signals from sensors or laboratory tests, and necessitate opening the package and sacrificing food samples. In contrast, colorimetric sensors target consumers or low-skilled professionals due to their relative ease of reading. Colorimetric sensors embedded into food packaging are expected to provide intuitive information of food quality and safety to final consumers without the need for user manuals or technical skills. Colorimetric sensors are generally considered less sensitive compared to fluorescence or electrochemical detection methods. However, polydiacetylene (PDA) liposomes have been extensively investigated due to the rapid color change (blue-to-red) and fluorescence generation induced by the conformational change of the backbone as a response to environmental perturbations such as heat, temperature, and mechanical pressure.^[22,23] To be used in sensors to target specific chemicals or microorganisms,^[24] PDA can be fabricated in the format of nano- or microliposomes and functionalized with various macromolecules such as carbohydrates,^[25] lipids,^[26] peptides,^[27] and antibodies.^[28,29] However, immobilization of colorimetric sensors on the inside of packaging material or in sachet limits the sensing efficacy to pathogens present on food surfaces and reduces the detection of pathogenic microorganisms that grow in microscopic cavities or inside food. Contamination of the interior food with the pathogenic microorganisms is often the case for various food products including meat, poultry, fish, and leafy greens,^[30] and is a growing public concern because the microorganisms cannot be removed by household washing.^[31,32] Contaminations then result in large food recalls and food waste, e.g., the romaine lettuce recall after an *E. coli* outbreak in 2018,^[16] which could be mitigated by having sensors that can effectively and easily detect presence of pathogens in food and that could be deployed in store or at home by consumers.^[33] Thus, there is a need to develop a new generation of colorimetric food sensors easily deployable and readable that can be used for food quality assurance and food safety.

Materials used for sensing in smart food labeling should be nontoxic and safe for oral consumption if they are in direct contact with food (which would correspond to a case-specific definition as Food Contact Substance of Generally Regarded as Safe (GRAS) by US Food and Drug Administration). In this regard, silk-based materials are emerging options for food contact applications as they are nontoxic and edible, possess tunable mechanical and chemical properties, and can be fabricated in several formats,^[34] including microneedles,^[35] screws,^[36] nanostructured films,^[37] and edible coatings.^[38] To add functions to the final material format, silk-materials can encapsulate and preserve active ingredients such as vitamins, antibiotics, antibodies, and bacteria within their structure.^[39] For example, an array of silk-based microneedles was used to encapsulate and deliver vaccines^[40] or to inject macromolecules in plants' vasculature for horizontal gene delivery.^[41] The mechanical strength of silk-based microneedles enabled application to hard plant tissues, which cannot be easily achieved by other microneedle injectors targeting soft dermis for drug delivery.^[42,43] For example, Cao et al. reported a silk microneedle with 0.4 N of tip breaking force that penetrated the stems of tomato (>0.03 N of penetration force) and delivered biomolecules to xylem (840–1040 μm of penetration depth).^[41] In another effort, PDA liposomes functionalized with an antibody for *E. coli* were ink-jet printed in a silk bioink^[34] on disposable gloves to sense

bacterial contamination on surfaces, although with low sensitivity and accuracy. Recently, advancement in synthetic biology of silk proteins have made significant progress and are opening the door to the scale-up production and commercialization of synthetic silk materials,^[44] possibly decreasing commercialization barriers for this material in food safety applications.

To address the sampling challenges intrinsic in colorimetric smart food labeling, we developed a silk-based technology that can both sample fluids deep in food tissues and render a colorimetric signal to indicate the presence or absence of pathogenic bacteria or food spoilage. We present a silk-based porous microneedle array with the backside printed with PDA liposomes, which can be functionalized with antibodies for bacterial sensing or left unfunctionalized to respond primarily to changes in sample pH. We demonstrate in situ detection of *E. coli*, used as a surrogate for pathogenic bacteria such as O157:H7, as well as food spoilage detected as an increase in food pH. The microneedles are strong enough to penetrate not only fish but also its packaging (i.e., commercial polyvinylidene chloride (PVDC) films). Once in contact with food, silk microneedles undergo poroelastic reswelling that causes the absorption of fluids and their transport to the backside, where the pathogen-specific colorimetric responses of the PDA liposomes are activated to develop unique color patterns that provide intuitive food safety and quality information.

2. Results and Discussion

2.1. Printing PDA Bioinks on Silk Microneedle Array for Colorimetric Detection of Food Pathogen and Spoilage

In **Figure 1**, we illustrate the proposed process for food pathogen and spoilage detection, from the fabrication of the silk microneedle array and the PDA bioinks to the colorimetric identification of food quality. To validate the idea, we fabricated a proof-of-concept device capable of detecting *E. coli* from fish fillets. Fabrication of both the microneedle array and the bioinks are based on silk fibroin regenerated from silkworm (*Bombyx mori*) cocoons. The extracted fibroin aqueous suspension is widely used to fabricate new biomaterials with pre-designed functions in multiple formats, such as solid, gel, or films.^{[45], [34]} For the preparation of PDA bioinks, diacetylene liposomes were synthesized from a solution containing 4:1 molar ratio of 10,12-pentacosadiynoic acid (PCDA) and 1,2-dimyristoyl-sn-glycero-3-phosphocholine (DMPC) as described in a previous study.^[29] DMPC was added as it has been shown that phospholipids incorporated within the liposomes increase the inks' detection sensitivity.^[26] DMPC also provides a binding site for horseradish peroxidase (HRP),^[46] which was conjugated with the *E. coli* targeting antibody by the manufacturer (ViroStat, #1094). The antibody, purified goat immune globulin G (IgG), was specific for "O" and "K" antigenic serotypes of *E. coli*, including serotype O157:H7. Silk fibroin, which is edible, performs as protective carriers to stabilize and preserve the PDA liposomes and antibodies^[29] after being printed on the backside of the silk microneedle arrays and exposed to environments.

An array of silk microneedles was obtained via replica molding using a negative poly(dimethyl siloxane) (PDMS)

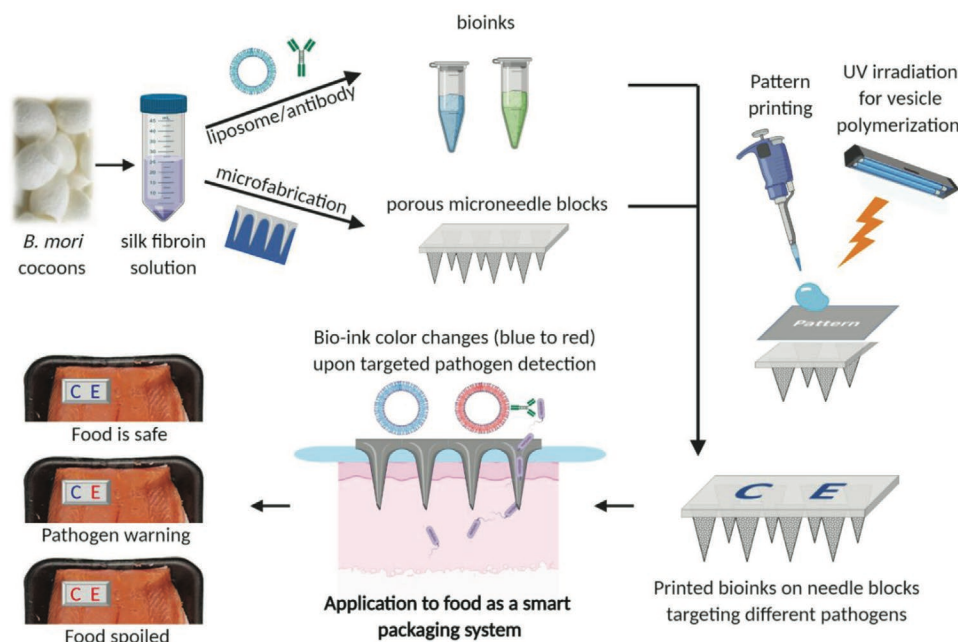


Figure 1. Schematic illustration of the proposed food quality monitoring system using silk microneedle arrays with printed bioinks as colorimetric sensors.

stamp. The array consists of conical needles (1600 μm in height, 600 μm in diameter, and 2 mm spacing between needles) that were long and strong enough to penetrate fish meat and commercial food wraps. The morphology of an individual needle cast from the mold is shown in Figure S1 in the Supporting Information. The PDA-based bioinks were drop cast on the backside of the needle arrays over a mask to create a text pattern. Printed inks were irradiated with UV-C light (254 nm) for 1-4-addition-polymerization to yield covalent connectivity between adjacent diacetylenes, forming PDA with an ene-yne alternating backbone structure.^[24] The blue color of the printed inks, which was developed during the polymerization, was expected to have chromatic change to red upon the immunocapture of *E. coli* and its antigens. For this study, we utilized two PDA bioinks without and with the antibody conjugation, which were printed in patterns “C” and “E,” representing “Control” and “*E. coli* targeting”, respectively. By comparing the color patterns developed from the letters, it is easy to assess the presence or absence of target bacteria.

2.2. Fabrication of Insoluble and Porous Needles

Controlling protein polymorphism of regenerative silk fibroin, as a technical material for food applications, enables the design of materials that can be stable in dry format in random coil or β -sheet structure, which in turn determines the end material properties such as solubility in water and mechanical strength.^[47] Water annealing (i.e., incubation in vacuum with water vapor^[48]) is considered as an appropriate method to modulate silk polymorphism for food application as it does not require any toxic solvent such as methanol.^[38] To decrease silk solubility in water and to increase fibrillar porous structure, we water annealed the needle arrays for 4–8 h after casting them in the PDMS mold. The apparent morphology of needles observed using optical microscopy did not change during water annealing (Figure 2A–C). However, electron micrographs taken at the cross-section of the needles depicted a clear increase in the formation of silk fibrils upon the random coil to β -sheet transition (Figure 2D,E), along with formation of

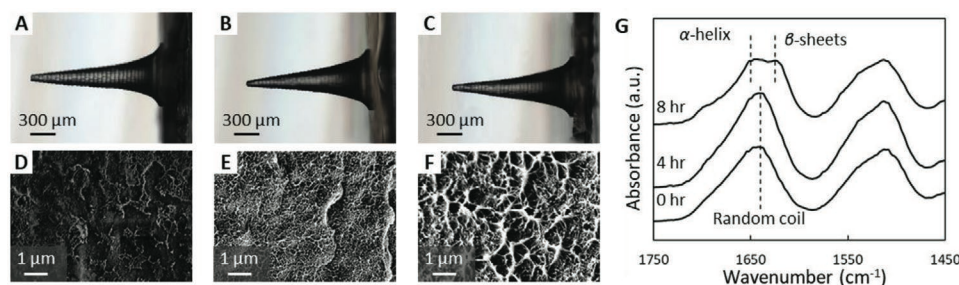


Figure 2. A–C) Optical images of silk needles. D–F) SEM images of cross-sectional areas of silk needles. Silk needles were water annealed for A,D) 0 h, B,E) 4 h, and C,F) 8 h. G) FTIR spectra of silk films after 0, 4, and 8 h of water annealing. Microscale pores are visible in (F), coincident with the transition between the random coil and helix-sheet conformations verified by FTIR.

pores.^[49] After 8 h of water annealing, the fibrillar structure was well-developed, creating pores larger than a few micrometers (Figure 2F), which were deemed to allow transport of *E. coli* in the silk structure. The formation of pores in the microneedles upon water annealing provided an opportunity to use their microstructure as a sampling device with enlarged surface area. Confined absorption of fluids by the needles upon insertion in food increase the flow of internal fluids via reswelling and capillary action within the pores and result in the diffusion of bacteria to the printed PDA inks. This process could be modeled with a Lucas–Washburn equation,^[41,50] although poroelastic models^[51] could also be applied to take into account the relaxation of the transient response of silk materials during reswelling, which enables the transport or diffusion of *E. coli* and their antigens through the microneedles. Formation of silk fibroin porous structures in microneedles upon water annealing was unexpected as this phenomenon is unreported for water annealed silk fibroin in a film format. Scanning electron microscopy (SEM) analysis of the top surface of silk films (≈ 50 μm thick) after 8 h of water annealing depicted a sample that is flat at the microscale (no distinguishable features are shown in Figure S2A in the Supporting Information). According to cross-sectional images of silk films analyzed by SEM, only a few local areas present a weakly fibrillar structure (Figure S2B, Supporting Information), while the majority of the sample appears flat with scattered sub-micrometer pores (Figure S2C, Supporting Information).

Additionally, we investigated changes in morphology of the microneedles using treatment in an 80% solution of ethanol overnight, which was designed to drive a higher degree of silk fibroin crystallization. Interestingly, no fibrillar porous structure was formed in the microneedles (Figure S2D,E, Supporting Information). Together, these results indicate that water annealing is an effective approach to develop a porous structure in silk microneedles. The water vapor-induced random coil to β -sheet transition of the protein involves both suspension (during rehydration) and condensation (during drying) of the silk material. These processes result in $\approx 12\%$ loss of free water and $\approx 10\%$ reduction in bulk density. As the shape and geometry of the needle is maintained during the process, the loss of material (water that is released and evaporates) results in the formation of pores. The phenomenon is less evident in thin silk films as the material collapses (reduction in thickness of a few percentages, depending on the width to length aspect ratio) during the water annealing process.

The amount of β -sheet structure induced during water annealing was quantified using Fourier-transform infrared spectroscopy (FTIR).^[47] The increase in crystallinity was evident as a peak at a wavenumber range of $1616\text{--}1637\text{ cm}^{-1}$, typical of β -sheet structure, appeared in the amide I region ($1595\text{--}1705\text{ cm}^{-1}$). A peak indicating α -helix structure (centered at circa 1660 cm^{-1}) may also develop during the transition from random coil to β -sheet. Fourier self-deconvolution analysis of the amide I region showed that β -sheet content increased from 17.5% to 20.7% and 29.8% after 4 and 8 h of water annealing, respectively (Figure 2G). The porous structure and the higher crystallinity of 8 h water annealed samples when compared to those of samples treated for 4 h were evident in SEM images (Figure 2E,F) and FTIR spectra, respectively. An additional

24 h of water annealing did not increase porosity significantly (Figure S2F, Supporting Information), indicating that the process plateaus at 8 h of water annealing. We then used the 8 h treated samples for the food experiments described below.

2.3. Polydiacetylene Liposome as a Colorimetric Biosensor for *E. coli* Detection

The efficacy of antibody conjugated PDA inks printed on silk was validated by measuring fluorescence intensity generated upon the contact with *E. coli* dispersed in phosphate buffer saline (PBS, pH 7.4). At a concentration of 10 nL IgG solution (10–20 ng of IgG) per mL of PDA ink, the difference in the fluorescence intensity between the PDA ink exposed to *E. coli* solution ($\text{OD}_{600} = 0.1$, $\approx 8 \times 10^7$ cells mL^{-1}) and PBS was the highest (Figure 3A), showing a continuous increase over a day (Figure 3B). With a higher IgG concentration, the fluorescence intensity from the ink decreased possibly due to the strong steric hindrance from among neighboring antibodies, preventing their association with *E. coli*.^[52] Figure 3C shows that the difference in this fluorescence intensity between PBS and *E. coli* solution was observed at $\text{OD}_{600} > 0.005$.

To have a proof-of-concept visualization of PDA color change in a food packaging phantom, 2 μL of PDA inks with different IgG concentrations were drop cast on a low-density polyethylene (LDPE) film, representing the inner side of a commercially available resealable food container. Then, the LDPE films were stored in petri-dishes with wet tissue paper that had been presoaked with *E. coli* dispersion in PBS. A distinct color change, evaluated by red chromaticity from RGB values of the images, was observed from the ink with 100 nL mL^{-1} IgG, while ink with no IgG remained blue (Figure 3D). A small portion of the ink with a lower concentration (10 nL mL^{-1}) turned to red. With higher concentrations ($1\text{ }\mu\text{L mL}^{-1}$), the printed ink showed somewhat a mixed response with blue and red colors visible in the pattern probably because of nonuniform distribution of antibodies or locally aggregation of PDA liposomes. The results indicate that the optimal IgG concentration depends on the choice of substrate upon which the ink is printed. In this study, the silk film required less optimal concentration of IgG than LDPE film (10 vs 100 nL mL^{-1}), possibly due to a superior capability of silk form for preserving biomolecules.^[39] However, for a fair comparison of the antibody preservation in different substrate may require additional experiments in future studies.

PDA generation of red fluorescence was also used to investigate sensor response and was imaged using fluorescence microscopy. Using nanoporous flexographic printing, we patterned the bioink (100 μm diameter circles with center to center distance of 130 μm) on a glass slide (Figure 3E).^[53,54] The glass slide with the printed PDA ink pattern was stored in a petri-dish with *E. coli* contaminated wet tissue paper. Then, a strong fluorescent signal was generated from the circular patterns, indicating *E. coli* detection by the antibodies conjugated with the PDA ink. The fluorescent intensity from *E. coli*-antibody reaction was comparable to positive control that was heat at 60°C , validating proper responses of the prepared PDA ink upon the detection of *E. coli* as a biosensor. While in this study, we focused our efforts on the use of colorimetric changes for

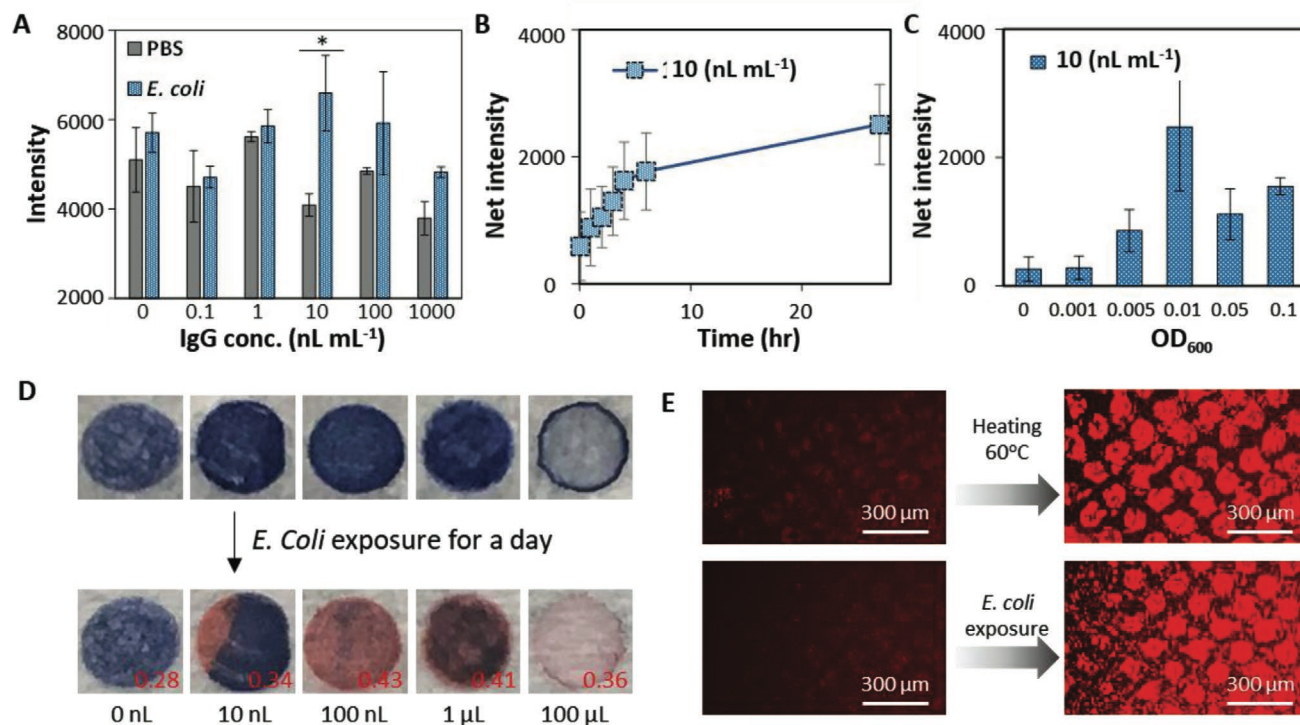


Figure 3. A) Fluorescence intensity from the PDA ink printed on silk film after 27 h exposure to PBS and *E. coli* containing solution ($OD_{600} = 0.1$). * indicates a statistical significance ($p < 0.1$, t -test). B) Net fluorescence intensity (intensity from *E. coli* solution – intensity from PBS) from the PDA ink (10 nL mL^{-1} IgG) as a function of exposure time. C) Net fluorescence intensity from the PDA ink (10 nL mL^{-1} IgG) as a function of *E. coli* concentration. D) Color and E) fluorescence changes of PDA inks when exposed to *E. coli*. The red numbers in (D) are red (R) chromaticity values calculated by dividing the R value by the sum of the R, green (G), and blue (B) values. The image process was conducted using an open source program, ImageJ. Error bars in (A)–(C) are standard deviations.

the development of a sensor that delivers straight forward information to low-skilled users without the need of any supporting devices, bioprinting of PDA ink using a nanoporous stamp showed promising results as a technique to precisely control the definition of biosensor patterns that can minimize the use of the ink and antibody.^[53,54] With assistance of small portable devices such as smartphone attachments to read and analyze fluorescence signals, the flexographic printing using the nanoporous stamp would be more easily accessible in the near future.^[21]

2.4. Food Sensing via Bioprinted Silk Needle Arrays and Films

We deployed the silk microneedle-based biosensor in hake fillet using a 4×2 array of needles with font size 12 pt letters “E” (consisting of bioink decorated with antibody targeting *E. coli*) and “C” (consisting of bioink without antibody) printed on the backside. Before the bioprinted needle arrays were applied, fish samples were precontaminated with *E. coli* in PBS. The results were also compared with samples treated with PBS or *Salmonella*-contaminated samples (Figure 4A). From the color patterns of the printed text, we provided three different modes of information to consumers. As a first pattern, both “C” and “E” letters maintained their blue colors originally developed by polymerization of the liposomes after UV exposure. This pattern indicates that the food is fresh and *E. coli* was not detected.

A second pattern corresponds to the change in blue to red only for “E,” indicating the detection of target pathogen, but that the food is not spoiled. The last pattern shows red colors for both “C” and “E,” which can be developed when the food is spoiled. For this study, fish was considered as spoiled when the pH of the fish, as a freshness indicator^[55], increased from an initial value of 7.0–7.3 to around 8.0 when unpleasant odor and loss of flesh elasticity were easily recognized. The changes in pH were similar for all samples regardless of the *E. coli* injection, indicating that the pH increase was mainly caused by degradation of muscle tissues by native microorganisms.^[56] At 16 h (before food was spoiled), only “E” showed red color change when exposed to *E. coli*, indicating that the color pattern can be used as food pathogen indicator. When the needle arrays were applied to uncontaminated or *Salmonella*-contaminated (nontargeting bacteria) fish, the color of printed texts remained blue, indicating specificity in the response of the sensor to different bacteria. For the detection of other pathogens, such as *Salmonella*, another bioink may be designed by changing the antibody used for detection. After 24 h, when the pH of the fish samples increased to around 8.0, all the texts printed showed a clear red color, indicating that samples were spoiled, regardless of the precontamination with pathogenic bacteria.

For comparison, the same letters were printed on the LDPE films (Figure 4B). Unlike the application of the needle array, where bioinks were printed on top of the array, the letters printed on the films were directly in contact with the fish fillet.

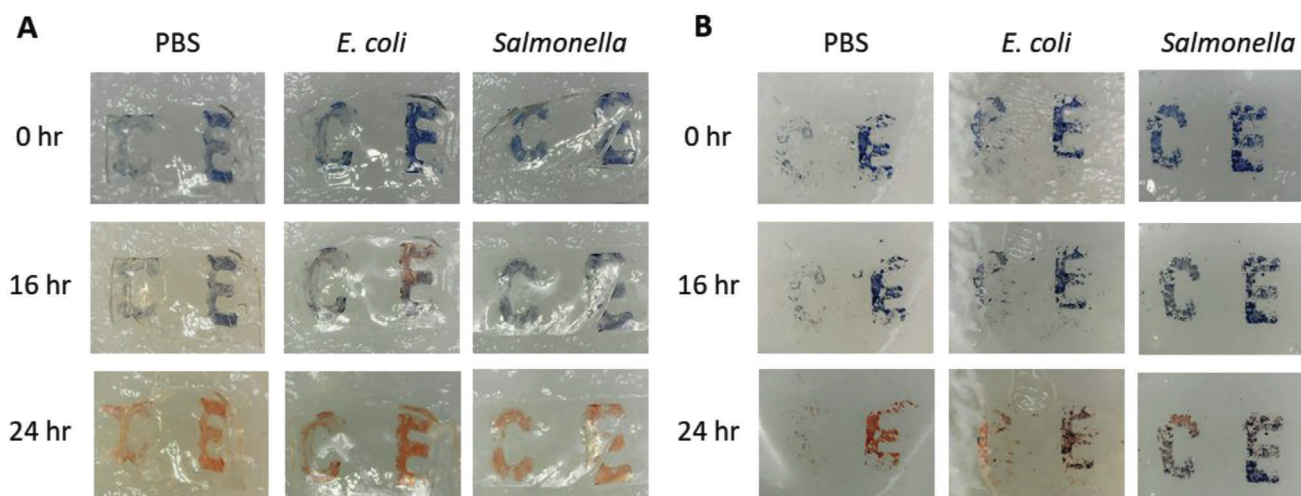


Figure 4. Fish application of PDA bioinks printed on A) silk microneedle arrays and B) LDPE films.

This limitation brought several disadvantages. First, the prints were easily damaged by shear force given to the film while being attached to the fish samples. However, the inks embedded in the silk needle arrays remained relatively stable due to the preserving ability of silk. Second, the contact between the ink and food samples is limited to the direct contact area only. On the other hand, the inks in the needle arrays are more evenly distributed within the porous structure of the needle increasing the contact area but resulting in a fainter blue color. In addition, the internal fluids can circulate through the porous structure as the evaporation of the water from the backside of the needle became the driving force to withdraw fluids in the fish samples. Therefore, the needle arrays showed faster color changes. With the film, the *E. coli* targeting inks missed detection of the pathogen (i.e., false negative reading) even at 16 h, when the change in the color of the sensor was not due to pathogen-specific contamination but to the basic pH upon spoilage. Lastly, the direct contact of the PDA bioink (or any other sensors) on the food would increase potential concerns about contamination of the food by the materials used for the ink. PDA is considered relatively safe with low cytotoxicity,^[57] and thus can be used as a drug carrier,^[58] however, its safety as a food contact substance is not fully demonstrated. The application of a material with GRAS status (as is silk fibroin) to transport food fluids to a sensing chemistry that does not come in contact with the food may open the door to more efficient and precise food monitoring systems. Nonetheless, future studies are required to fully

ensure the stability of the bioink printed on the microneedle array and the possible migration of PDA to the food tissue.

Another advantage of using silk-needle arrays is that the sensor can be deployed through the food packaging, without the need to open it. **Figure 5A** shows that silk microneedles are robust enough to penetrate commercial PVDC food wrap. The films were applied to spoiled haddock fillets wrapped in the food film (Figure 5B), showing a clear color change within 4 h (Figure 5C) as the internal fluid of the fish was transported from the flesh to the printed bioink through the porous structure within the needle and across the packaging.

3. Outlook

In this study, we presented a proof-of-concept sensor that consists of a sampling unit that can transport inner food fluids to a colorimetric bioinks for detection of food spoilage and pathogens. The silk-based porous needle array described here is made of an edible, nontoxic material and has been designed to facilitate the exposure of the sensing component with inner fluids present in food, contributing to a faster response and enabling the detection of pathogenic bacterial present in food. At the same time, the array of microneedles mediates an indirect contact between the food and the sensing bioink, enabling material contact only between an edible protein, such as silk fibroin, and the food and hindering

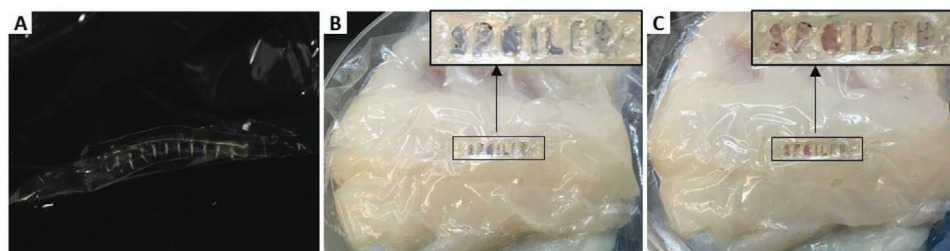


Figure 5. A) A silk microneedle array penetrating a commercial food wrap. Application to detecting spoiled haddock fillet through the food packaging materials at B) 0 h and C) 4 h. Insets in (B) and (C) are zoomed-in images of the needle arrays.

possible exposure to the sensing component. This advantage may increase the options of materials and chemistries used in the synthesis of the bioinks, reducing technical barriers to develop sensors with improved sensitivity and selectivity. At the same time, the use of edible materials may alleviate customers' concerns on the use of new engineered materials in contact with food. Moreover, the mechanical strength of the needles, which was enough to penetrate commercial food wrap, allowed the sensor to be used easily without opening the package. The simple change of color in printed patterns may allow consumers to recognize food information intuitively without the aid of further instruments. The PDA bioink described here may also be coupled with printing technologies so that multiple pathogen-specific inks can be delivered on a substrate in patterns that can be interrogated with portable devices and interpreted remotely.^{[19],[20],[21]} Flexographic printing using nanoporous stamp,^[53,54] as introduced in this study, or inkjet printing^[29] can be a promising option. Future research may focus on the improved modification of PDA bioinks so that they can be universally applied to different foods (varying pH) and storage conditions (varying temperature). Improvement of the pore structure may enhance the transport of target pathogens or molecules into the inks. Investigation of the 3D pore-structure using computer-aided tomographic technology and the transport of fluids with varying viscosity (simulating different types of foods) through the pores would be helpful to optimize the structures. Improved sensor materials and microneedles with optimized pore structure based on the platform introduced in this study will result in a sensitive, rapid-acting sensor that can be deployed at various points along the supply chain.

4. Experimental Section

Preparation of Silk Fibroin Solution: The regenerated silk fibroin was extracted from *B. mori* cocoons following an established protocol.^[45] In brief, pieces of silk cocoons ($\approx 2 \times 2 \text{ cm}^2$) were boiled in 0.02 M sodium carbonate solution for 30 min to remove the sericin, an adhesive protein coating the core silk fibers. The obtained degummed silk fibers were then washed with ultrapure water (18.2 M Ω cm) for several times followed by overnight drying. The dried silk fibers were dissolved in 9.3 M lithium bromide for 4 h at 60 °C followed by dialysis against ultrapure water in a dialysis cassette (molecular weight cut-off: 3500 Da) for 2 days with frequent replacements. The resulting silk fibroin solution was then centrifuged to remove impurities (at 4800 \times g, 20 min \times 2). The final silk fibroin solution was diluted with water to 6 wt%, and then stored at 4 °C until use.

Preparation of Bioink as a Colorimetric Sensor: The bioink consisted of antibody conjugated PDA liposomes, and silk fibroins were prepared based on a method described in a previous study^[29] and elsewhere.^[59,60] As a diacetylene lipid monomer solution, 10×10^{-3} M PCDA (Sigma-Aldrich) was dissolved in chloroform. In a separate bottle, 10×10^{-3} M of DMPC (Sigma-Aldrich) was also prepared in chloroform. Then, PCDA (2 mL) and DMPC (0.5 mL) solutions were mixed and dried under a chemical fume hood. The dried PCDA:DMPC mixture was redispersed in water (12.5 mL) using a sonifier (Branson SFX 550, 1/2 in. microtip) under a pulsed ultrasonication (10 s on and off, total pulse duration 10 min \times 3, amplitude ≈ 80 W out power). The ultrasonicated solution (2×10^{-3} M of PCDA/DMPC mixture at 4:1 molar ratio) was filtered through 0.45 μm cellulose acetate syringe filter to yield $\approx 800 \mu\text{g mL}^{-1}$ PCDA/DMPC liposomes. Goat IgG (ViroStat, #1094, conjugated with

HRP by manufacturer) as an antibody targeting *E. coli* (0–1 μg) was added to 1 mL filtered PCDA:DMPC solution. The solution was then incubated at 4 °C overnight to conjugate the phospholipid with the antibody through an HRP-mediated reaction. H_2O_2 (0.3%) and copper sulfate (30×10^{-6} M) were added to deactivate excessive HRP. Finally, silk fibroin solution was added to be 0.005 wt% of the solution to provide necessary stabilization of embedded IgG without excessive constraints for conformation changes in the PDA upon stimuli. Safety note: Chloroform is hazardous via inhalation, highly painful through skin contact, and permeates nitrile gloves. Chloroform-containing solutions should only be handled in a fume hood. When pouring chloroform, or in other circumstances where there is a risk of significant spillage, gloves such as polyvinyl acetate or SilverShield are recommended. Plastic shatterproof vessels are recommended for use during probe sonication.

Preparation of Silk Microneedle Array and Bioink Printing: The silk microneedle array was fabricated using a negative mold made of PDMS (Sylgard 184, Dow-Corning). The negative PDMS mold was prepared by casting the materials over aluminum master mold, degassing, and incubating at 70 °C for 2 h as described in the recent study.^[41] The silk fibroin solution was added to the PDMS mold, followed by centrifuge at 2000 rcf for 5 min. The mold was kept in a fume hood at 100 feet min^{-1} to dry overnight at room temperature. After being peeled off from the mold, the cast needle array was water annealed by exposing it to water vapors under vacuum at room temperature following protocols described elsewhere.^[48] For bioprinting, PDA (2 μL) ink was drop cast on a piece of microneedle array covered by a mask. The mask was prepared by laser cutting the adhesive tape sheet (3M, 200 MP). After drying, printed inks were irradiated with UV-C light (254 nm) for 5 min for polymerization of PDA. During curing, the UV source (Analytic Jena 3UV Lamp 3UV-38, 8 W) was placed at a height of ≈ 3 cm above the printed sample.

Nanoporous Stamp Fabrication, Inking, and Printing: To fabricate the stamps,^[53] first vertically aligned CNT arrays (CNT “forests”) were grown on lithographically patterned silicon substrates by atmospheric pressure chemical vapor deposition (CVD). Then, the top entangled “crust” layer ($< 1 \mu\text{m}$ thickness) was removed by a brief oxygen plasma etching (Diener, Femto Plasma System) and coated with a thin layer (≈ 20 nm) of poly-perfluorodecylacrylate (pPFDA) using initiated CVD (iCVD).^[53,61,62] The plasma etching was critical to remove the stiff and rough crust, which was undesirable for high-resolution printing because it might result in nonuniform contact against the target substrate. The pPFDA coating followed by second plasma treatment allowed liquid infiltration and solvent evaporation without shrinkage or collapse of the CNT forest by elastocapillary densification. The final plasma-treated pPFDA-CNT microstructures were highly porous ($> 90\%$ porosity) with nanometer pore size (≈ 100 – 200 nm), and allowed liquid infiltration without deformation due to capillary forces. These structures were mechanically compliant and uniformly contacted with the target substrates. A 500 μL droplet of the bioink was pipetted onto the stamp and then the stamp was spun to 1500 rpm for 45–60 s in a spincoater. The inked stamp contacted against the target substrate under a contact pressure of ≈ 50 – 100 kPa and then retracted leaving the printed pattern on the substrate. After drying, printed PDA inks were polymerized as conducted for inks on silk microneedle arrays.

Characterization of Silk Microneedle Array: The optical images of individual silk needles and the fluorescence images of flexographically printed micropattern were obtained with a microscope (Nikon Eclipse TE2000-E). Cross-sectional images of porous silk needles were imaged by SEM (Zeiss Merlin High-resolution SEM). The samples were freeze-dried (FreeZone, LABCONCO), mechanically broken, and then sputter coated with gold for 10 nm before imaging. FTIR spectrometer (Spectrum 65, Perkin Elmer) was used to evaluate the crystallinity of silk films. Spectra were collected at a wavelength range of 4000 to 650 cm^{-1} , with a resolution of 4 cm^{-1} and an accumulation of 64 scans. The relative fractions of different secondary structures (random coil, α -helix, and β -sheet) of silk fibroins were determined by Fourier self-deconvolution of the Amide I band (1705–1595 cm^{-1}) and Gaussian curve-fitting of the deconvoluted spectra using the software, Origin 8.1 Pro.

Fluorescence Intensity: For the optimization of antibody concentration, 5 μL of inks with varying IgG concentrations (0–1000 nL IgG solution (ViroStat, #1094) per 1 mL of filtered vesicle suspension, IgG concentration in the solution was 1–2 mg mL⁻¹) were drop cast on silk films on a 96 well-plate followed by UV-C light irradiation (254 nm) for 5 min. The silk films were prepared by drop casting 50 μL of 6% silk fibroin solution in the plate, followed by drying and water annealing. For the generation of fluorescence by the interplay between antibody and antigen, *E. coli* (ATCC 25922, a nonpathogenic surrogate of O157:H7^[63]) was cultured in a trypticase soy broth (ATCC Medium 18) until the solution's optical density measured by light absorbance at a wavelength of 600 nm (OD₆₀₀) reached over 0.2. Then, *E. coli* was centrifuged at 14 000 rcf for 5 min \times 2 and redispersed in PBS (OD₆₀₀ = 0.1, $\approx 8 \times 10^7$ cells mL⁻¹). Then *E. coli* suspension in PBS (100 μL) was added to each well of the plate. The increased fluorescence intensity (excitation 520 nm, emission 590 nm) from printed inks in the plate was monitored over time using a Tecan microplate reader.

Food Application: Fresh hake (*Merluccius albidus*, a species of fish in the family of cod-like fish, Merlucciidae) and haddock (*Melanogrammus aeglefinus*, a family member of the Gadidae, which is known as the cods) fillets were purchased from a local fish market in Cambridge, MA. Before applying the preprinted microneedle array, the fillets, cut into ≈ 30 g pieces, were precontaminated by the injection of 1 mL *E. coli* resuspended PBS (OD₆₀₀ = 0.1). PBS without bacterium and PBS with resuspended *Salmonella enterica* (ATCC 53648, Le Minor and Popoff serovar Typhimurium) were also injected to fish samples for comparison. The color change of the bioink was monitored by taking images of the array using a portable USB digital microscope (Jiusion).

Supporting Information

Supporting Information is available from the Wiley Online Library or from the author.

Acknowledgements

This work was supported by the Abdul Latif Jameel Water & Food Systems (J-WAFS) at the Massachusetts Institute of Technology, Office of Naval Research (Award No. N000141812258, B.M.), and the National Science Foundation (Award No. CMMI-1752172, B.M.). A.J.H. and D.M. also acknowledge the National Science Foundation (CMMI-1826216). This work made use of the Shared Experimental Facilities supported in part by the MRSEC program of the National Science Foundation (DMR-1419807). The authors also acknowledge use of facilities of the Institute for Soldier Nanotechnologies (ISN) at the Massachusetts Institute of Technology.

Conflict of Interest

The authors declare no conflict of Interest.

Keywords

bacterial detection, colorimetric sensors, food safety, polydiacetylene liposome, silk

Received: June 25, 2020

Revised: July 25, 2020

Published online: September 9, 2020

[1] H. Yousefi, H. M. Su, S. M. Imani, K. Alkhalidi, C. D. Filipe, T. F. Didar, *ACS Sens.* **2019**, *4*, 808.

- [2] World Health Organization, Food safety, <https://www.who.int/news-room/fact-sheets/detail/food-safety> (accessed: August 2020).
- [3] Centers for Disease Control and Prevention, CDC and Food Safety, <https://www.cdc.gov/foodsafety/cdc-and-food-safety.html> (accessed: August 2020).
- [4] H. C. J. Godfray, J. R. Beddington, I. R. Crute, L. Haddad, D. Lawrence, J. F. Muir, J. Pretty, S. Robinson, S. M. Thomas, C. Toulmin, *Science* **2010**, *327*, 812.
- [5] D. Hoover, L. Moreno, *Estimating Quantities and Types of Food Waste at the City Level*, New York, NY, USA **2017**.
- [6] A. L. Brody, B. Bugusu, J. H. Han, C. K. Sand, T. H. McHugh, *J. Food Sci.* **2008**, *73*, R107.
- [7] Economics of Traceability for Mitigation of Food Recall Costs, <https://mpra.ub.uni-muenchen.de/id/eprint/27677> (accessed: August 2020).
- [8] A. D. Sezer, Ç. Haksöz, *Math. Oper. Res.* **2012**, *37*, 399.
- [9] M. M. Aung, Y. S. Chang, *Food Control* **2014**, *39*, 172.
- [10] C. Rukchon, A. Nopwinyuwong, S. Trevanich, T. Jinkarn, P. Suppakul, *Talanta* **2014**, *130*, 547.
- [11] C. M. P. Yoshida, V. B. V. Maciel, M. E. D. Mendonça, T. T. Franco, *LWT—Food Sci. Technol.* **2014**, *55*, 83.
- [12] J. Fernández-Salmerón, A. Rivasdeneyra, M. A. C. Rodríguez, L. F. Capitan-Vallvey, A. J. Palma, *IEEE Sens. J.* **2015**, *15*, 5726.
- [13] Y. Galagan, W. F. Su, *Food Res. Int.* **2008**, *41*, 653.
- [14] B. G. Werner, J. L. Koontz, J. M. Goddard, *Curr. Opin. Food Sci.* **2017**, *16*, 40.
- [15] V. P. Romani, V. G. Martins, J. M. Goddard, *Food Control* **2020**, *109*, 106946.
- [16] T. Bintsis, *AIMS Microbiol.* **2018**, *4*, 377.
- [17] B. B. Dzantiev, N. A. Byzova, A. E. Urusov, A. V. Zherdev, *TrAC, Trends Anal. Chem.* **2014**, *55*, 81.
- [18] L. Zheng, G. Cai, W. Qi, S. Wang, M. Wang, J. Lin, *ACS Sens.* **2020**, *5*, 65.
- [19] H. Yousefi, M. M. Ali, H. M. Su, C. D. M. Filipe, T. F. Didar, *ACS Nano* **2018**, *12*, 3287.
- [20] S. Li, J. Liu, Z. Chen, Y. Lu, S. S. Low, L. Zhu, C. Cheng, Y. He, Q. Chen, B. Su, Q. Liu, *Sens. Actuators, B* **2019**, *297*, 126811.
- [21] H. Zhu, U. Sikora, A. Ozcan, *Analyst* **2012**, *137*, 2541.
- [22] B. Yoon, S. Lee, J. M. Kim, *Chem. Soc. Rev.* **2009**, *38*, 1958.
- [23] J. Park, S. K. Ku, D. Seo, K. Hur, H. Jeon, D. Shvartsman, H. K. Seok, D. J. Mooney, K. Lee, *Chem. Commun.* **2016**, *52*, 10346.
- [24] E. Cho, S. Jung, *Molecules* **2018**, *23*, 107.
- [25] B. Ma, Y. Fan, L. Zhang, X. Kong, Y. Li, J. Li, *Colloids Surf., B* **2003**, *27*, 209.
- [26] K. W. Kim, H. Choi, G. S. Lee, D. J. Ahn, M. K. Oh, *Colloids Surf., B* **2008**, *66*, 213.
- [27] S. Song, K. Ha, K. Guk, S. G. Hwang, J. M. Choi, T. Kang, P. Bae, J. Jung, E. K. Lim, *RSC Adv.* **2016**, *6*, 48566.
- [28] S. Kolusheva, R. Yossef, A. Kugel, M. Katz, R. Volinsky, M. Welt, U. Hadad, V. Drory, M. Kliger, E. Rubin, A. Porgador, R. Jelinek, *Anal. Chem.* **2012**, *84*, 5925.
- [29] H. Tao, B. Marelli, M. Yang, B. An, M. S. Onses, J. A. Rogers, D. L. Kaplan, F. G. Omenetto, *Adv. Mater.* **2015**, *27*, 4273.
- [30] J. A. Neal, E. Cabrera-Diaz, A. Castillo, *Agric., Food Anal. Bacteriol.* **2012**, *2*, 275.
- [31] A. May, USA Today, <https://www.usatoday.com/story/news/health/2018/11/21/romaine-lettuce-warning-you-cant-wash-off-e-coli/2077052002/> (accessed: August 2020).
- [32] E. Uhlig, C. Olsson, J. He, T. Stark, Z. Sadowska, G. Molin, S. Ahrné, B. Alsanusi, Å. Håkansson, *Food Sci. Nutr.* **2017**, *5*, 1215.
- [33] CDC Food Safety Alert: *E. coli* Outbreak Linked to Romaine Lettuce, <https://www.cdc.gov/media/releases/2018/s1120-ecoli-romain-lettuce.html> (accessed: August 2020).
- [34] B. Marelli, N. Patel, T. Duggan, G. Perotto, E. Shirman, C. Li, D. L. Kaplan, F. G. Omenetto, *Proc. Natl. Acad. Sci. USA* **2017**, *114*, 451.

- [35] K. Tsioris, W. K. Raja, E. M. Pritchard, B. Panilaitis, D. L. Kaplan, F. G. Omenetto, *Adv. Funct. Mater.* **2012**, 22, 330.
- [36] G. S. Perrone, G. G. Leisk, T. J. Lo, J. E. Moreau, D. S. Haas, B. J. Papenburg, E. B. Golden, B. P. Partlow, S. E. Fox, A. M. S. Ibrahim, S. J. Lin, D. L. Kaplan, *Nat. Commun.* **2014**, 5, 3385.
- [37] O. Rathore, D. Y. Sogah, *Macromolecules* **2001**, 34, 1477.
- [38] B. Marelli, M. A. Brenckle, D. L. Kaplan, F. G. Omenetto, *Sci. Rep.* **2016**, 6, 25263.
- [39] A. T. Zvinashe, E. Lim, H. Sun, B. Marelli, *Proc. Natl. Acad. Sci. USA* **2019**, 116, 25555.
- [40] J. A. Stinson, W. K. Raja, S. Lee, H. B. Kim, I. Diwan, S. Tutunjian, B. Panilaitis, F. G. Omenetto, S. Tzipori, D. L. Kaplan, *ACS Biomater. Sci. Eng.* **2017**, 3, 360.
- [41] Y. Cao, E. Lim, M. Xu, J.-K. Weng, B. Marelli, *Adv. Sci.* **2020**, 7, 1903551.
- [42] P. Singh, A. Carrier, Y. Chen, S. Lin, J. Wang, S. Cui, X. Zhang, *J. Controlled Release* **2019**, 6, 1612.
- [43] K. J. Lee, Y. Xue, J. Lee, H. J. Kim, Y. Liu, P. Tebon, E. Sarikhani, W. Sun, S. Zhang, R. Haghniaz, B. Çelebi-Saltik, X. Zhou, S. Ostrovidov, S. Ahadian, N. Ashammakhi, M. R. Dokmeci, A. Khademhosseini, *Adv. Funct. Mater.* **2020**, 30, 2000086.
- [44] A. Scott, *Chem. Eng. News* **2014**, 92, 24.
- [45] D. N. Rockwood, R. C. Preda, T. Yücel, X. Wang, M. L. Lovett, D. L. Kaplan, *Nat. Protoc.* **2011**, 6, 1612.
- [46] M. B. Fritzen-Garcia, V. C. Zoldan, I. R. W. Z. Oliveira, V. Soldi, A. A. Pasa, T. B. Creczynski-Pasa, *Biotechnol. Bioeng.* **2013**, 110, 374.
- [47] X. Hu, D. Kaplan, P. Cebe, *Macromolecules* **2006**, 39, 6161.
- [48] X. Hu, K. Shmelev, L. Sun, E. S. Gil, S. H. Park, P. Cebe, D. L. Kaplan, *Biomacromolecules* **2011**, 12, 1686.
- [49] H. Sun, B. Marelli, *Nat. Commun.* **2020**, 11, 351.
- [50] E. W. Washburn, *Phys. Rev.* **1921**, 17, 273.
- [51] Y. Li, T. Tanaka, *J. Chem. Phys.* **1990**, 92, 1365.
- [52] J. U. Lee, J. H. Jeong, D. S. Lee, S. J. Sim, *Biosens. Bioelectron.* **2014**, 61, 314.
- [53] S. Kim, H. Sojoudi, H. Zhao, D. Mariappan, G. H. McKinley, K. K. Gleason, A. J. Hart, *Sci. Adv.* **2016**, 2, e1601660.
- [54] D. D. Mariappan, S. Kim, M. S. H. Boutilier, J. Zhao, H. Zhao, J. Beroz, U. Muecke, H. Sojoudi, K. Gleason, P.-T. Brun, A. J. Hart, *Langmuir* **2019**, 35, 7659.
- [55] K. A. Abbas, A. Mohamed, B. Jamilah, M. Ebrahimian, *Am. J. Biochem. Biotechnol.* **2008**, 4, 614.
- [56] L. Gram, H. H. Huss, *Int. J. Food Microbiol.* **1996**, 33, 121.
- [57] X. Yan, X. An, *Nanoscale* **2013**, 5, 6280.
- [58] C. Guo, S. Liu, Z. Dai, C. Jiang, W. Li, *Colloids Surf., B* **2010**, 76, 362.
- [59] D. H. Kang, H. S. Jung, J. Lee, S. Seo, J. Kim, K. Kim, K. Y. Suh, *Langmuir* **2012**, 28, 7551.
- [60] C. P. de Oliveira, N. D. F. F. Soares, E. A. F. Fontes, T. V. de Oliveira, A. M. M. Filho, *Food Chem.* **2012**, 135, 1052.
- [61] M. Gupta, K. K. Gleason, *Langmuir* **2006**, 22, 10047.
- [62] H. Sojoudi, S. Kim, H. Zhao, R. K. Annavarapu, D. Mariappan, A. J. Hart, G. H. McKinley, K. K. Gleason, *ACS Appl. Mater. Interfaces* **2017**, 9, 43287.
- [63] J. K. Kim, M. A. Harrison, *J. Food Prot.* **2009**, 72, 1385.